Progress In Electromagnetics Research B, Vol. 54, 245–264, 2013

PHYSICS-BASED EXPANSION ON 3D CONFORMAL GAUSSIAN BEAMS FOR THE SCATTERING FROM A CURVED INTERFACE

Alexandre Chabory [1, 2, *], Jérôme Sokoloff [3, 4], and Sylvain Bolioli [5]

[1]ENAC, TELECOM-EMA, F-31055 Toulouse, France

[2]Université de Toulouse, F-31400 Toulouse, France

[3]Université de Toulouse, UPS, INPT, LAPLACE (Laboratoire Plasma et Conversion d'Energie), 118 route de Narbonne, F-31062 Toulouse Cedex 9, France

[4]CNRS, LAPLACE, F-31062 Toulouse, France

[5]Onera — The French Aerospace Lab, F-31055 Toulouse, France

Abstract—Gaussian beams techniques are high-frequency asymptotic methods that can be used to model the propagation/interaction of fields in a variety of problems. In this article, an expansion is proposed to express the scattering of magnetic/electric currents from a curved interface in terms of a new kind of elementary beams, the conformal Gaussian beams. The expansion characteristics rely on the physical properties of the configuration, which leads to represent the scattering with a small number of conformal Gaussian beams. An analytical formulation for the conformal Gaussian beams is developed, which expression is derived from an asymptotic evaluation of the radiation integrals valid at great distance from the interface. An example is presented to show that this analytical formulation is in good agreement with the reference result. Numerical tests are led on the expansion in order to show that the scattering can be represented with accuracy by adding the contribution of conformal Gaussian beams.

Received 11 July 2013, Accepted 28 August 2013, Scheduled 6 September 2013

* Corresponding author: Alexandre Chabory (alexandre.chabory@recherche.enac.fr).

1. INTRODUCTION

Gaussian beams have first been introduced in laser-optics [1] before being used in the domain of optical and quasi-optical systems. They now constitute widely-developed tools for many applications in high-frequency computational electromagnetics. They can be employed in the analysis of metallic reflectors [2, 3], lenses [4], radomes [5, 6], rough surfaces [7], dichroic surfaces [8], or propagation channels [9]. There are generally two key components in a modeling approach based on Gaussian beams: the expansion and the tracking. Expansion techniques allow for the representation of fields as sums of elementary beams. Tracking techniques deal with the propagation/interaction of elementary beams in the environment, e.g., the interaction of beams with dielectric and metallic interfaces.

A large family of expansions already exists for Gaussian beams. Among them, the multimodal orhtogonal Gauss-Hermite and Gauss-Laguerre bases were first introduced in laser-optics [1]. They were subsequently applied in electromagnetics by taking into account vectorial fields [10]. However, these expansions suffer from a strong limitation, the paraxial approximation, that imposes to describe fields weakly diverging with respect to a main propagation direction. That is the reason why other approaches have been investigated. The Gabor bases and frames allow for the representation of a signal in terms of Gaussian functions placed on a doubly infinite discrete spectral-spatial lattice. In electromagnetics, Gabor expansions have been used to express the radiation from a planar surface as a sum of beams shifted both in position and in propagation direction [11]. Other beam expansions have recently been proposed that are based on the generalized pencil of function method (GPOF) [12].

In many applications, the initial surface on which the field is known may be curved. This is particularly the case for conformal antennas, radomes, or metallic reflectors. To treat such cases, one possibility is to keep the multimodal orthogonal bases [2, 13]. On the other hand, new specific expansions dedicated to initial curved surfaces can also be developed. In [5], we have developed a pragmatic expansion to express a field known on a moderately curved surface as a set of equally spaced Gaussian beams. The expansion characteristics have been chosen from the physical properties of the configuration. Numerical experiments have demonstrated the efficiency of this approach. However, limitations exist that concern the incidence of the initial field, and the curvature of the surface, which both must remain moderate.

In order to overcome these limitations, we have used the Gabor

frames to expand electric and magnetic currents on a regular curved interface in dimension 2 [14]. This expansion has required the introduction of a new class of beams, the conformal Gaussian beams (CGB). They correspond to the radiation of elementary currents which have a Gaussian amplitude and linear phase, both with respect to the curvilinear coordinate of the curve. We have developed an analytical formulation for such beams valid at great distances. Nevertheless, the number of beams generated within this expansion may become very large because of the doubly spatial-spectral Gabor lattice. To reduce this number, we have modified this approach by taking into account the physical properties of the configuration [15]. The extension of this technique to 3D configurations has first been introduced in [16]. Further, analytical formulations for the plane wave spectrum of a 3D CGB have been derived in [17].

In this article, we present and test an approach to represent the radiation of currents from a curved surface as a sum of CGB in 3D. As for the 2D case [15], we employ the physical properties of the configuration to define the expansion characteristics. Indeed, the curvature of the surface and the main radiation directions of the currents are locally taken into account. An analytical formulation for 3D CGB is developed from an asymptotic evaluation of the radiation integrals valid at large distances of the surface.

We start by presenting the principles and characteristics of the expansion in Section 2. We develop an analytical formulation and we give an example of a conformal Gaussian beam in Section 3. Few numerical experiments are led to demonstrate the capabilities of our expansion in Section 4.

2. PHYSICS-BASED EXPANSION

2.1. Principle of the Expansion

We consider a regular surface (S) splitting the space into two regions 1 and 2 (Fig. 1). On a limited section of (S), we assume that there are electric and/or magnetic surface currents $(\mathbf{J}, \mathbf{M})$. As for the 2D case presented in [15], our aim is to represent the radiation of these currents as a superposition of a finite number of elementary beams.

At any point $\mathbf{r}'$ of (S), $\mathbf{n}$ stands for the unit normal vector oriented from 1 to 2. Because $\mathbf{J}(\mathbf{r}')$ and $\mathbf{M}(\mathbf{r}')$ are tangent to (S), they can be written as the sum of two orthogonal components, i.e.,

$$\begin{aligned} \mathbf{J} &= J^a \boldsymbol{\tau}^a + J^b \boldsymbol{\tau}^b, \\ \mathbf{M} &= M^a \boldsymbol{\tau}^a + M^b \boldsymbol{\tau}^b, \end{aligned} \tag{1}$$

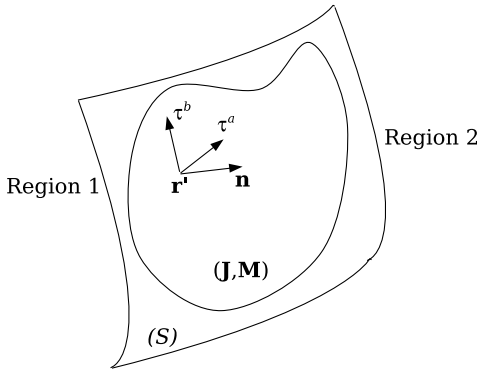

Figure 1. Initial 3D configuration.

in which $\boldsymbol{\tau}^a$ and $\boldsymbol{\tau}^b$ are two unitary tangent vectors such that $(\boldsymbol{\tau}^a, \boldsymbol{\tau}^b, \mathbf{n})$ is orthonormal and direct. From an arbitrary constant unitary vector $\boldsymbol{\tau}^0$, that respects $\boldsymbol{\tau}^0 \neq \mathbf{n}$ for any $\mathbf{r}' \in (S)$, we choose

$$\boldsymbol{\tau}^a\left(\mathbf{r}'\right) = \frac{\mathbf{n}\left(\mathbf{r}'\right) \times \boldsymbol{\tau}^0}{\left\|\mathbf{n}\left(\mathbf{r}'\right) \times \boldsymbol{\tau}^0\right\|}, \quad \boldsymbol{\tau}^b\left(\mathbf{r}'\right) = \mathbf{n}\left(\mathbf{r}'\right) \times \boldsymbol{\tau}^a\left(\mathbf{r}'\right). \tag{2}$$

The expansion of the electric and magnetic currents on N elementary currents can be written as

$$\begin{aligned} \mathbf{J}\left(\mathbf{r}'\right) &= \sum_{\alpha=a,b} \sum_{n=1}^{N} a_n^{J\alpha} u_n(\mathbf{r}') \boldsymbol{\tau}^{\alpha}(\mathbf{r}'), \\ \mathbf{M}\left(\mathbf{r}'\right) &= \sum_{\alpha=a,b} \sum_{n=1}^{N} a_n^{M\alpha} u_n(\mathbf{r}') \boldsymbol{\tau}^{\alpha}(\mathbf{r}'), \end{aligned} \tag{3}$$

where $a_n^{J\alpha}$ and $a_n^{M\alpha}$ represent the expansion coefficients, and u_n stands for the expansion functions. From (3), the expansion of the currents $(\mathbf{J}, \mathbf{M})$ can be reduced to the expansion of 4 scalar components. We obtain explicitly

$$K = \sum_{n=1}^{N} a_n^K u_n, \quad \text{for } K = J^a, J^b, M^a, M^b. \tag{4}$$

We want to choose the expansion functions u_n in the same way as for the 2D cases studied in [14, 15]. In these articles, this choice originated in the Gabor bases/frames. These functions had a Gaussian-amplitude and linear-phase, both with respect to the curvilinear coordinate of the curve from which the expansion was performed. This becomes

irrelevant here because the expansion is performed from a surface. To overcome this difficulty, we firstly associate with each elementary current n a reference frame $(\mathbf{c}_n, \boldsymbol{\tau}_n^a, \boldsymbol{\tau}_n^b, \mathbf{n}_n)$. This reference frame is constituted by a point $\mathbf{c}_n$ in (S), and by the vectors $(\boldsymbol{\tau}^a, \boldsymbol{\tau}^b, \mathbf{n})$ evaluated at $\mathbf{c}_n$, i.e.,

$$\boldsymbol{\tau}_n^a = \boldsymbol{\tau}^a(\mathbf{c}_n), \quad \boldsymbol{\tau}_n^b = \boldsymbol{\tau}^b(\mathbf{c}_n) \quad \mathbf{n}_n = \mathbf{n}(\mathbf{c}_n). \tag{5}$$

In this reference frame, the coordinates of $\mathbf{r}'$ are denoted (x'_n, y'_n, z'_n). Secondly, to be consistent with [14, 15], u_n is expected to have a Gaussian-amplitude linear-phase evolution. This evolution is here related to the transverse coordinates x'_n and y'_n. It can be obtained by means of the formulation

$$u_n\left(x'_n, y'_n\right) = u_0 \exp\left(-\frac{jk}{2}\begin{bmatrix} x'_n \\ y'_n \end{bmatrix}^T \mathbf{Q}_n^f \begin{bmatrix} x'_n \\ y'_n \end{bmatrix} - j\boldsymbol{\beta}_n^T \begin{bmatrix} x'_n \\ y'_n \end{bmatrix}\right), \tag{6}$$

where $j = \sqrt{-1}$, k is the wavenumber and the phase vector $\boldsymbol{\beta}_n$ introduces the linear phase term. Further, $\mathbf{Q}_n^f$ is the complex curvature matrix associated with the n-th current. To insure the Gaussian evolution of the amplitude, its imaginary part must be negative definite. At any point $\mathbf{r}$, the fields radiated by $(\mathbf{J}, \mathbf{M})$, can be expressed as the sum of the fields radiated by each elementary currents. This yields the field expansion

$$\begin{aligned} \mathbf{E}(\mathbf{r}) &= \sum_{K=J^a,\ldots,M^b} \sum_{n=1}^{N} a_n^K \mathbf{E}_n^K(\mathbf{r}), \\ \mathbf{H}(\mathbf{r}) &= \sum_{K=J^a,\ldots,M^b} \sum_{n=1}^{N} a_n^K \mathbf{H}_n^K(\mathbf{r}), \end{aligned} \tag{7}$$

in which $(\mathbf{E}_n^K, \mathbf{H}_n^K)$ represent the electric and magnetic fields radiated by the n-th current of type K. These elementary fields define the conformal Gaussian beams (CGB) for 3D configurations. These new beams, which properties will be studied in Section 3, can be regarded as an extension of the beams proposed for 2D configurations in [14, 15].

2.2. Choice of the Expansion Characteristics

In the expansion presented in the previous section, three parameters need to be specified. The first one is the position of the beam centres $\mathbf{c}_n$, from which the beam reference frames can be obtained via (5). The two others characterize u_n, they are the curvature matrix $\mathbf{Q}_n^f$, and the phase vector $\boldsymbol{\beta}_n$. To obtain an accurate description of the

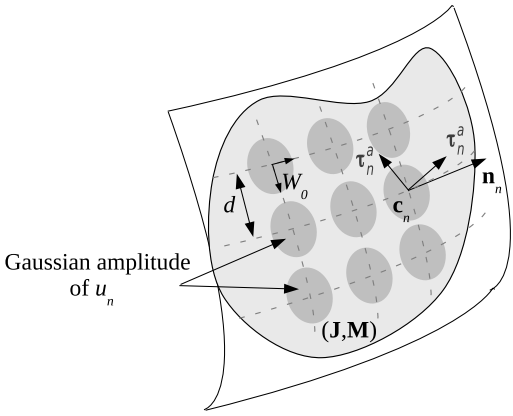

Figure 2. Choice of $\mathbf{c}_n$ and $\mathbf{Q}_n^f$.

currents ($\mathbf{J}$, $\mathbf{M}$) with as few elementary beams as possible, we adopt a pragmatic approach that uses the physics of the configuration, and that is similar to the ones exposed in [5, 15].

The beam centres $\mathbf{c}_n$ are equally spaced on the surface (S). Hence, they are placed on a regular mesh of size d of (S) (Fig. 2). The number of expansion functions N corresponds to the number of mesh points. The spatial homogeneity of the beam centre distribution leads to choose $\mathbf{Q}_n^f$ independently of n, and to employ symmetric Gaussian functions. This yields the choice

$$\mathbf{Q}_n^f = \mathbf{Q}^f = -\frac{2j}{kW_0^2}\begin{bmatrix}1 & 0\\ 0 & 1\end{bmatrix} \quad \text{for} \quad n = 1, \ldots, N, \tag{8}$$

where W_0 represents the Gaussian waist.

The choice of $\boldsymbol{\beta}_n$ follows from the local physical properties of the currents ($\mathbf{J}$, $\mathbf{M}$). The n-th expansion function u_n should describe as precisely as possible these currents near the point $\mathbf{c}_n$. Hence, we impose to u_n the same phase evolution as the initial currents locally near $\mathbf{c}_n$. This can be realized by employing the phase derivative of the initial currents at $\mathbf{c}_n$ [15]. However, in practical applications the numerical values of the phase derivatives may not be simply computable. This is particularly the case when the initial currents are only known at the points $\mathbf{c}_n$. Another choice for $\boldsymbol{\beta}_n$ is possible in configurations for which the problem is specified only in terms of fields. The fields ($\mathbf{E}$, $\mathbf{H}$) are known on (S), and the expansion aims at representing their radiation by means of CGB in region 2. In such a case, the currents to be

expanded can be obtained from the equivalence theorem, which states

$$\begin{aligned} \mathbf{J} &= \mathbf{n} \times \mathbf{H}, \\ \mathbf{M} &= -\mathbf{n} \times \mathbf{E}. \end{aligned} \tag{9}$$

These currents radiate zero in region 1 and ($\mathbf{E}$, $\mathbf{H}$) in region 2. As it will be illustrated in Section 3, for $\|\boldsymbol{\beta}_n\| < k$, a CGB mainly propagates in one direction in region 1 and one direction in region 2. In the reference frame ($\mathbf{c}_n$, $\boldsymbol{\tau}_n^a$, $\boldsymbol{\tau}_n^b$, $\mathbf{n}_n$). These directions are symmetric with respect to the local tangent plane at $\mathbf{c}_n$. They correspond to the vectors

$$\begin{aligned} &\left[\beta_n^a \quad \beta_n^b \quad \sqrt{k^2 - {\beta_n^a}^2 - {\beta_n^b}^2}\right]^T && \text{in region 2,} \\ &\left[\beta_n^a \quad \beta_n^b \quad -\sqrt{k^2 - {\beta_n^a}^2 - {\beta_n^b}^2}\right]^T && \text{in region 1.} \end{aligned} \tag{10}$$

Note that similar expressions exist for the 2D case [15]. Hence, $\boldsymbol{\beta}_n$ can be chosen so that, locally near $\mathbf{c}_n$, the n-th CGB and the fields propagate in the same direction in region 2. This choice can be expressed by means of the Poynting vector of ($\mathbf{E}$, $\mathbf{H}$) evaluated at $\mathbf{c}_n$ as

$$\beta_n^\alpha = k \frac{\mathbf{P}(\mathbf{c}_n) \cdot \boldsymbol{\tau}_n^\alpha}{\|\mathbf{P}(\mathbf{c}_n)\|} \quad \text{for } \alpha = a, b \tag{11}$$

in which $\mathbf{P}(\mathbf{c}_n)$ is the Poynting vector at $\mathbf{c}_n$, i.e.,

$$\mathbf{P} = \frac{1}{2} \mathbb{R}\mathrm{e}(\mathbf{E} \times \mathbf{H}^*). \tag{12}$$

Note that to compute $\boldsymbol{\beta}_n$ with (11), only the numerical values of ($\mathbf{E}$, $\mathbf{H}$) at $\mathbf{c}_n$ are needed.

As to conclude, for $\mathbf{c}_n$ and $\mathbf{Q}_n^f$, the choice has been reduced to two distances: the mesh size d, and the Gaussian width W_0. A discussion based on a numerical experiment will be conducted in Section 4 to estimate satisfying values for these parameters. For $\boldsymbol{\beta}_n$, we have proposed an expression, (11), based on the local properties of the initial currents.

2.3. Computation of the Expansion Coefficients

As in [5, 15], a point matching technique is employed in order to compute the expansion coefficients a_n^K. The expressions (4) are discretized on the points $\mathbf{c}_p$ for $p = 1, \ldots, N$, which yields the 4 following linear systems

$$K(\mathbf{c}_p) = \sum_{n=1}^{N} a_n^K u_n(\mathbf{c}_p) \quad \text{for} \quad K = J^a, J^b, M^a, M^b. \tag{13}$$

On a matricial point of view, these systems can be written as

$$\mathbf{A}\mathbf{x}^K = \mathbf{b}^K \quad \text{for } K = J^a, J^b, M^a, M^b \tag{14}$$

in which the matrix $\mathbf{A}$ is given by

$$(\mathbf{A})_{p,n} = u_n(\mathbf{c}_p) \quad \text{for } p, n = 1, \ldots, N. \tag{15}$$

Further, $\mathbf{x}^K$ and $\mathbf{b}^K$ represent vectors containing the unknown coefficients and the current K sampled at $\mathbf{c}_p$, respectively. They can be expressed as

$$\mathbf{x}^K = \left[a_1^K, \ldots, a_N^K\right]^T \quad \text{for } K = J^a, J^b, M^a, M^b, \tag{16}$$

and

$$\mathbf{b}^K = [K(\mathbf{c}_1), \ldots, K(\mathbf{c}_N)]^T \quad \text{for } K = J^a, J^b, M^a, M^b. \tag{17}$$

Note that the 4 linear systems use the same matrix $\mathbf{A}$ with 4 different right-hand-sides. Therefore, they can efficiently be solved with only one LU decomposition of $\mathbf{A}$.

3. THE CONFORMAL GAUSSIAN BEAMS

3.1. Analytical Formulation

In the previous section, an expansion has been proposed to express currents on a surface as a superposition of elementary Gaussian-amplitude linear-phase currents. To compute the radiated fields as a sum of conformal Gaussian beams via (7), we develop here analytical expressions for these beams.

In this section, we consider one CGB characterized by its centre $\mathbf{c}_0$, its curvature matrix $\mathbf{Q}^f$, and its linear phase vector $\boldsymbol{\beta}_0$ (Fig. 3). We remind that the CGB reference frame ($\mathbf{c}_0$, $\boldsymbol{\tau}_0^a$, $\boldsymbol{\tau}_0^b$, $\mathbf{n}_0$) is defined by (5).

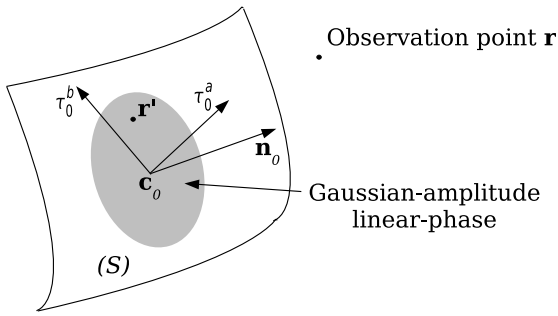

Figure 3. One conformal Gaussian beam.

Here, coordinates will be expressed in this reference frame. To develop an analytical expression for the beam, an analytic description of the way (S) evolves near the point $\mathbf{c}_0$ is required. This can be obtained using a second-order approximation from which (S) is characterized by its curvature matrix Q^S computed at $\mathbf{c}_0$. Within this approximation, the coordinates $(x',\, y',\, z')$ of $\mathbf{r}' \in (S)$ respect the relation

$$z' = -\frac{1}{2}\begin{bmatrix} x' \\ y' \end{bmatrix}^T \mathbf{Q}^S \begin{bmatrix} x' \\ y' \end{bmatrix}. \tag{18}$$

At any observation point $\mathbf{r}$ such that $r = \|\mathbf{r}\|$ is greater than few wavelengths, the CGB expressions are given, for $\alpha = a,\, b$, by

$$\begin{aligned}
\mathbf{E}^{M^\alpha}(\mathbf{r}) &= jk \int_S \left[\mathbf{r}_1 \times \mathbf{M}^\alpha(\mathbf{r}')\right] G\left(\mathbf{r}-\mathbf{r}'\right) d\mathbf{r}', \\
\mathbf{H}^{M^\alpha}(\mathbf{r}) &= \frac{jk}{Z_0} \int_S \left[\mathbf{r}_1 \times \left(\mathbf{r}_1 \times \mathbf{M}^\alpha\left(\mathbf{r}'\right)\right)\right] G\left(\mathbf{r}-\mathbf{r}'\right) d\mathbf{r}', \\
\mathbf{E}^{J^\alpha}(\mathbf{r}) &= jkZ_0 \int_S \left[\mathbf{r}_1 \times \left(\mathbf{r}_1 \times \mathbf{J}^\alpha\left(\mathbf{r}'\right)\right)\right] G\left(\mathbf{r}-\mathbf{r}'\right) d\mathbf{r}', \\
\mathbf{H}^{J^\alpha}(\mathbf{r}) &= -jk \int_S \left[\mathbf{r}_1 \times \mathbf{J}^\alpha\left(\mathbf{r}'\right)\right] G\left(\mathbf{r}-\mathbf{r}'\right) d\mathbf{r}',
\end{aligned} \tag{19}$$

where Z_0 is the wave impedance in free space, and

$$\mathbf{r}_1 = \frac{\mathbf{r}-\mathbf{r}'}{\|\mathbf{r}-\mathbf{r}'\|}, \quad G\left(\mathbf{r}-\mathbf{r}'\right) = \frac{e^{-jk\|\mathbf{r}-\mathbf{r}'\|}}{4\pi\,\|\mathbf{r}-\mathbf{r}'\|}. \tag{20}$$

The expressions of the fields in (19) are all similar. From now on, for the sake of clarity, we will only develop the formulation associated with $\mathbf{E}^{M^\alpha}$. From the surface approximation (18), $d\mathbf{r}'$ can be formulated in terms of dx' and dy' as

$$d\mathbf{r}' = \|\mathbf{N}\| dx' dy' \quad \text{with} \quad \mathbf{N} = \begin{bmatrix} [x' & y'] \mathbf{Q}^S & 1 \end{bmatrix}^T. \tag{21}$$

Consequently, the radiation integral for $\mathbf{E}^{M^\alpha}$ in (19) can be approximated by

$$\mathbf{E}^{M^\alpha} = \int_{-\infty}^{+\infty} \int_{-\infty}^{+\infty} \mathbf{f}\left(x', y'\right) e^{g(x',y')} dx' dy', \tag{22}$$

in which

$$\mathbf{f}\left(x', y'\right) = \frac{u_0 jk \|\mathbf{N}\|}{4\pi\,\|\mathbf{r}-\mathbf{r}'\|} \mathbf{r}_1 \times \boldsymbol{\tau}^\alpha, \tag{23}$$

and

$$g(x', y') = -\frac{jk}{2}\begin{bmatrix} x' \\ y' \end{bmatrix}^T \mathbf{Q}^f \begin{bmatrix} x' \\ y' \end{bmatrix} - j\boldsymbol{\beta}_0^T \begin{bmatrix} x' \\ y' \end{bmatrix} - jk\left\|\mathbf{r}-\mathbf{r}'\right\|. \tag{24}$$

The integral in (22) has the suitable form for an asymptotic evaluation by the steepest descent path method [18]. In order to determine the saddle points of $g(x', y')$ defined by $\partial_{x'} g(x'_s, y'_s) = \partial_{y'} g(x'_s, y'_s) = 0$, we perform a second order approximation on $\|\mathbf{r}-\mathbf{r}'\|$. This approximation, denoted as the large distance approximation, assumes that $r \gg r'$ but is however not as strict as the classical far-field approximation. It yields

$$\left\|\mathbf{r}-\mathbf{r}'\right\| \approx r + \frac{1}{2}\begin{bmatrix} x' \\ y' \end{bmatrix}^T \left(\mathbf{Q}^{int} + \cos\theta \mathbf{Q}^S\right) \begin{bmatrix} x' \\ y' \end{bmatrix} - \frac{xx'+yy'}{r} \tag{25}$$

where $\cos\theta = \mathbf{r}\cdot\mathbf{n}_0$ and $\mathbf{Q}^{int}$ is the intermediate matrix

$$\mathbf{Q}^{int} = \frac{1}{r}\begin{bmatrix} 1-\frac{x^2}{r^2} & -\frac{xy}{r} \\ -\frac{xy}{r} & 1-\frac{y^2}{r^2} \end{bmatrix}. \tag{26}$$

Replacing $\|\mathbf{r}-\mathbf{r}'\|$ by (25) in (24), we find one single saddle point

$$\begin{bmatrix} x'_s \\ y'_s \end{bmatrix} = -\frac{1}{k}\mathbf{Q}^{-1}\xi \tag{27}$$

with

$$\mathbf{Q} = \mathbf{Q}^{int} + \mathbf{Q}^f + \cos\theta \mathbf{Q}^S, \tag{28}$$

and

$$\xi = \boldsymbol{\beta}_0 - \frac{k}{R}\begin{bmatrix} x \\ y \end{bmatrix}. \tag{29}$$

Finally, the steepest descent path method combined with the large distance approximation provides an analytical expression for $\mathbf{E}^{M^\alpha}$ given by

$$\mathbf{E}^{M^\alpha}(\mathbf{r}) = U(\mathbf{r})\, \mathbf{r}_{1s} \times \boldsymbol{\tau}_s^\alpha \tag{30}$$

in which the function $U(\mathbf{r})$ is defined by

$$U(\mathbf{r}) = \frac{\|\mathbf{N}_s\|}{2\|\mathbf{r}-\mathbf{r}'_s\|}\frac{u_0}{\sqrt{\det\mathbf{Q}}}\exp\left(\frac{j}{2k}\xi^T\mathbf{Q}^{-1}\xi - jkr\right). \tag{31}$$

Furthermore, $\mathbf{r}'_s$ is the point of coordinates (x'_s, y'_s, z'_s), with z'_s given by (18), and $\boldsymbol{\tau}_s^\alpha$, $\mathbf{r}_{1s}$, $\mathbf{N}_s$ correspond to (2), (20), and (21) evaluated at $\mathbf{r}'_s$.

A similar approach can be used for the other radiation integrals in (19). Upon assuming the large distance approximation, this yields the following analytical formulations

$$\begin{aligned} \mathbf{E}^{M^\alpha}(\mathbf{r}) &= U(\mathbf{r})\mathbf{r}_{1s} \times \boldsymbol{\tau}_s^\alpha, \\ \mathbf{H}^{M^\alpha}(\mathbf{r}) &= \frac{U(\mathbf{r})}{Z_0}\mathbf{r}_{1s} \times (\mathbf{r}_{1s} \times \boldsymbol{\tau}_s^\alpha), \end{aligned} \tag{32}$$

and

$$\begin{aligned}\mathbf{E}^{J^\alpha}(\mathbf{r}) &= Z_0 U(\mathbf{r})\mathbf{r}_{1s} \times (\mathbf{r}_{1s} \times \boldsymbol{\tau}_s^\alpha),\\ \mathbf{H}^{J^\alpha}(\mathbf{r}) &= -U(\mathbf{r})\mathbf{r}_{1s} \times \boldsymbol{\tau}_s^\alpha,\end{aligned} \tag{33}$$

for $\alpha = a, b$. Concerning the validity of these analytical expressions, the large distance approximation that is employed here is less demanding than the far-field approximation. For a beam with a Gaussian amplitude of width W_0, the far-field approximation holds for $r \gg kW_0^2/2$ [14].

In [17], the analytical plane wave spectrum of conformal Gaussian beams has been derived, which has allowed for a far-field formulation. Upon assuming $r \to +\infty$ in (32) and (33), we obtain the far-field expressions proposed in this article, i.e.,

$$\begin{aligned}\mathbf{E}^{M^\alpha} &= U(\mathbf{r})\hat{\mathbf{r}} \times \boldsymbol{\tau}_n^\alpha,\\ \mathbf{H}^{M^\alpha} &= \frac{U(\mathbf{r})}{Z_0}\hat{\mathbf{r}} \times (\hat{\mathbf{r}} \times \boldsymbol{\tau}_n^\alpha),\end{aligned} \tag{34}$$

and

$$\begin{aligned}\mathbf{E}^{J^\alpha} &= Z_0 U(\mathbf{r})\hat{\mathbf{r}} \times (\hat{\mathbf{r}} \times \boldsymbol{\tau}_n^\alpha),\\ \mathbf{H}^{J^\alpha} &= -U(\mathbf{r})\hat{\mathbf{r}} \times \boldsymbol{\tau}_n^\alpha,\end{aligned} \tag{35}$$

with $\hat{\mathbf{r}} = \mathbf{r}/r$, and

$$U(\mathbf{r}) = \frac{u_0}{2\sqrt{\det \mathbf{Q}}} \exp\left(\frac{j}{2k}\xi^T \mathbf{Q}^{-1}\xi\right) \frac{\exp(-jkr)}{r}. \tag{36}$$

Besides, for $\mathbf{Q}^S = 0$, $\boldsymbol{\beta}_0 = 0$, this expression corresponds to the far-field formulation of the fundamental Gaussian beam [5]. Nevertheless, it is difficult to relate conformal Gaussian beams to other kinds of Gaussian beams, e.g., the fundamental paraxial mode or the complex source point, because there are several major differences. Firstly, the sources that radiate a CGB are not localized at infinity, but on a known curved surface (S). Secondly, the asymptotic evaluation presented here is not based on the standard paraxial or far-field approximations, but on a large-distance approximation.

3.2. Example of a Conformal Gaussian Beam

In this section, we illustrate the properties of conformal Gaussian beams, and we test their large-distance formulation. We consider a beam such that $K = M^a$ (i.e., associated with magnetic currents

oriented along $\boldsymbol{\tau}^a$) and with parameters

$$\mathbf{Q}^f = -\frac{j}{kW_0^2}\begin{bmatrix}1 & 0\\ 0 & 1\end{bmatrix}, \quad \boldsymbol{\beta}_0 = \begin{bmatrix}k\sin\frac{\pi}{3}\\ 0\end{bmatrix},$$

$$W_0 = 2\lambda, \qquad \mathbf{Q}^S = \begin{bmatrix}\frac{-1}{20\lambda} & 0\\ 0 & \frac{-1}{10\lambda}\end{bmatrix}.$$

In Fig. 4, we display the beam amplitude in the near field zone obtained with the large-distance formulation (32), and the numerical computation of the radiation integral (19). Both results present a good agreement for values of $\mathbf{r}$ greater than few λ, i.e., at large distances from the beam centre. As expected, the field propagates with a limited spatial spread along one direction in region 1 and one direction in region 2. These two main propagation directions of the CGB are predicted in (10). They form here angles of $\pi/3$ and $2\pi/3$ with respect to $\mathbf{n_0}$. We also notice that due to the interface curvature $\mathbf{Q}^S$, the fields in region 1 and 2 are not strictly the same.

The validity of the analytical formulation is confirmed by Fig. 5, in which we display the difference between the reference electric field and the large-distance formulation. This result, which estimates the accuracy of the analytical expression, remains everywhere below $-30\,\mathrm{dB}$ for $r > 5\lambda$. Next, in Fig. 6, we analyze the CGB in the far-field zone on the complete 3D sphere, and also on the plane $y = 0$. In this simulation, the large-distance approximation perfectly holds, and hence the analytical formulation matches with the reference solution. Note also that the finite angular spread of the CGB with respect to its two main propagation directions appears clearly in this figure.

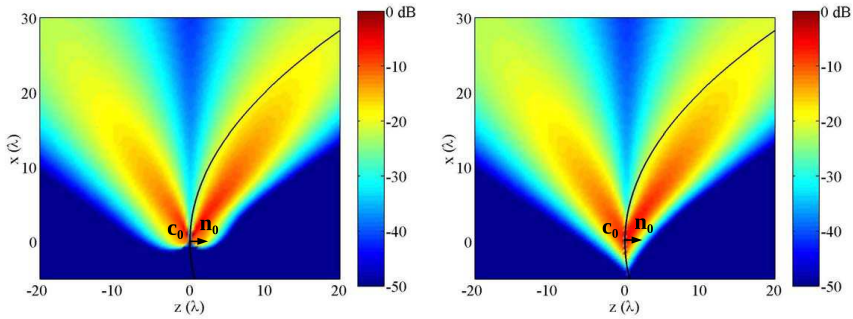

Figure 4. Electric field of a CGB near (S): (a) large-distance formulation, (b) reference.

4. NUMERICAL EXPERIMENTS: EXPANSION ON A ELLIPSOIDAL INTERFACE

4.1. Configuration

In this section, we discuss a few numerical experiments with the expansion technique. The geometry of the configuration is depicted in Fig. 7. The surface S is ellipsoidal of semi axes 15λ, 20λ, 25λ. We consider the field $\mathbf{E}$, $\mathbf{H}$ radiated from electrical and magnetic sources located on a planar aperture at $z = 5\lambda$. These sources are defined by

$$\mathbf{J}_s = \frac{f(x,y)}{Z_0}\mathbf{x}, \quad \mathbf{M}_s = f(x,y)\mathbf{y}, \tag{37}$$

where

$$f(x,y) = \begin{cases} \cos\frac{\pi\sqrt{x^2+y^2}}{L} & \text{for } \sqrt{x^2+y^2} \leq L/2, \\ 0 & \text{elsewhere.} \end{cases} \tag{38}$$

The aperture diameter L is set to 10λ. Our numerical experiments consist in expanding $\mathbf{E}$, $\mathbf{H}$ on (S) via the equivalent currents (9).

4.2. Choice of the Expansion Parameters

We start our analysis with $d = W_0 = \lambda$. On the part of the ellispoid where the equivalent currents are not negligible, the mesh contains 3670 points $\mathbf{c}_n$, hence the expansion is performed using $N = 3670$ beams. To determine $\boldsymbol{\beta}_n$, we use the Poynting vector of $\mathbf{E}$, $\mathbf{H}$ at $\mathbf{c}_n$ acccording to (11). In Fig. 8, we represent the equivalent magnetic currents on S obtained by summing all the elementary contributions in (3). We note

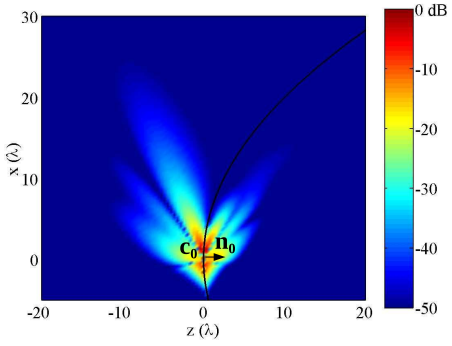

Figure 5. Difference between the reference and the analytical formulation of the electric field.

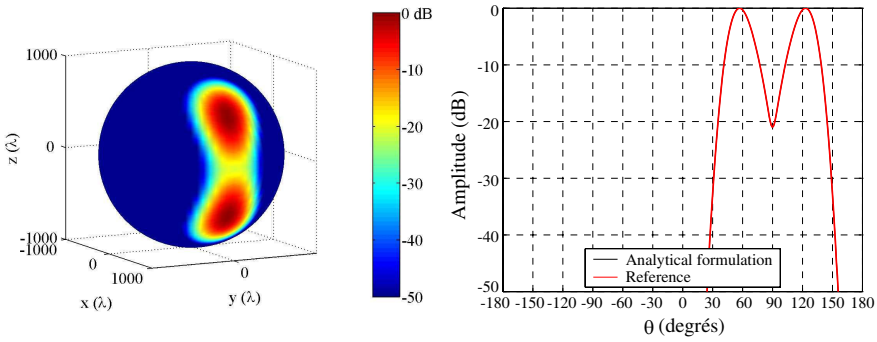

Figure 6. Normalized electric far-field of a CGB: (a) sphere at $r = 1000\lambda$, (b) plane $y = 0$ at $r = 1000\lambda$.

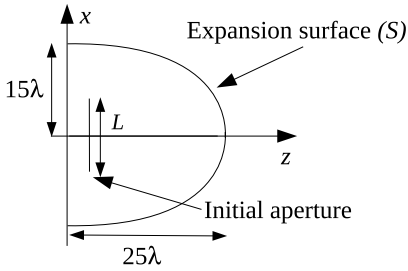

Figure 7. Configuration for the numerical experiment.

a very good agreement with the initial equivalent current since the difference is everywhere below -50 dB. In this example, the minimal and maximal values of $\|\boldsymbol{\beta}_n\|$ are 0 and $0.9k$. Besides, the diagonal terms of $\mathbf{Q}_n^S$, that describe the local surface curvature, vary from $1/(9\lambda)$ to $1/(41.5\lambda)$. This shows how the local properties of the configuration influences the beam parameters.

For the choice of d and W_0, we can rely on the study led in [15] for 2D configurations. In this study, limits in the choice of d and the ratio $\kappa = d/W_0$ have been estimated by means of a theoretical comparison with the use of Gabor frames [14]. Besides, these limits have been confirmed by numerical simulations. Following these results, we can expect an accurate expansion for a mesh size d between 0.5λ and few λ, and for a ratio $\kappa = d/W_0$ such that $0.5 \leq \kappa \leq 2$.

In order to check the influence of varying the expansion parameters, we introduce a number that measures the accuracy of the

expansion. It is defined as the root mean square error of the currents on S, i.e.,

$$\sigma^2 = \frac{\int_S Z_0^2 \|\mathbf{J_e} - \mathbf{J}\|^2 + \|\mathbf{M_e} - \mathbf{M}\|^2 dS}{\int_S Z_0^2 \|\mathbf{J}\|^2 + \|\mathbf{M}\|^2 dS}. \tag{39}$$

where $\mathbf{J}$, $\mathbf{M}$ and $\mathbf{J_e}$, $\mathbf{M_e}$ represent the initial equivalent currents and the expanded currents (3), respectively. In the experiments performed in this section, a threshold of $\sigma_{\mathrm{dB}} < -30\,\mathrm{dB}$ is chosen to estimate whether the expansion works correctly. In Fig. 9(a), we display σ for various values of d and κ. For small and large values of κ, we observe

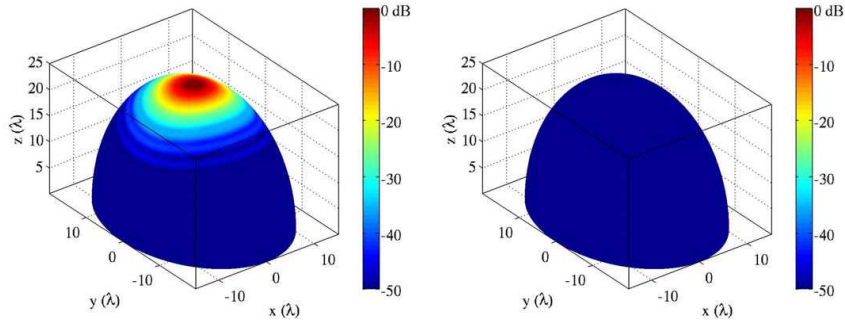

Figure 8. Magnetic current on the interface: (a) summation according to (1), (b) difference with the reference.

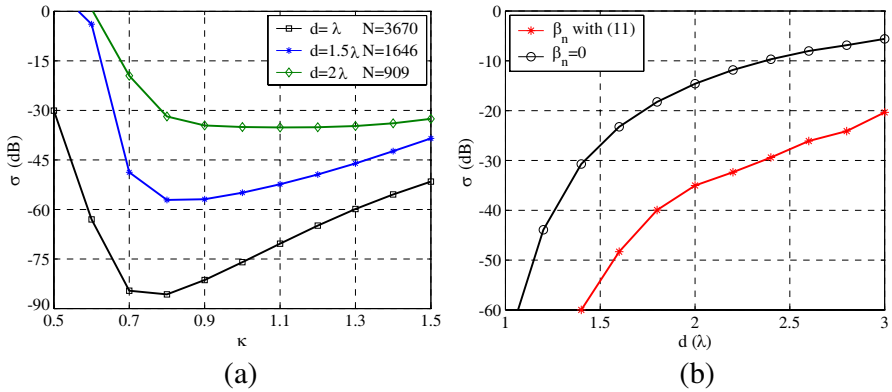

Figure 9. Role of the expansion parameters on the expansion accurary: (a) influence of d and $\kappa = d/W_0$, (b) influence of d and $\boldsymbol{\beta}_n$.

more important errors, corresponding to a less efficient description of the currents. For small values of κ, the points $\mathbf{c}_n$ are near, thus the expansion functions u_n overlay strongly and the coupling becomes too strong. For large values of κ, the distance between the points $\mathbf{c}_n$ is large, hence the expansion functions u_n are sparsely distributed and they are unable to describe the currents between the points $\mathbf{c}_n$. This refines the statement for the choice of κ, i.e., satisfying results are obtained for $0.8 \leq \kappa \leq 1.5$ in the worst case of Fig. 9(a).

Further, we note that σ decreases when d decreases. This may be explained by the fact that d determines the mesh size and consequently the number of expansion functions. With small values of d, the accuracy is improved because the currents are described with more expansion functions.

We now test the efficiency of (11) to determine the phase term $\boldsymbol{\beta}_n$ of the functions u_n. In Fig. 9(b), we compare the formulation (11) with $\boldsymbol{\beta}_n = 0$, which corresponds to orient the propagation axis of the beam at $\mathbf{c}_n$ along the normal $\mathbf{n}_n$. Since the Poynting vectors add physical information in the expansion functions, the formulation (11) improves significantly the expansion accurracy, specially for large values of d when less expansion functions are employed.

4.3. Influence of the Configuration

In the next simulation, we experiment the expansion in various configurations for $\kappa = 1$ and $d = 1.5\lambda$. In order to analyze how the field and the surface S play a role in the expansion accuracy, we modify the ellispoid semi-axis with respect to z and we consider two other laws $f(x, y)$ for the excitation. These laws are given by

$$f(x,y) = \begin{cases} 1 & \text{for } \sqrt{x^2+y^2} \leq L/2, \\ 0 & \text{elsewhere,} \end{cases} \tag{40}$$

and

$$f(x,y) = \exp\left(-\frac{x^2+y^2}{W^2}\right), \quad \text{with } W = 2\lambda. \tag{41}$$

In Fig. 10, we display the error σ in the various configurations. We observe that the Gaussian law leads to neglectable expansion errors regardless of the semi-axis length. Therefore, the expansion remains accurate even when the local incidence is increased and when the surface presents significant variations in its curvature. With the cosine law, the error remains below the threshold of $-30\,\mathrm{dB}$. Nevertheless, σ becomes slightly more important when the semi-axis is decreased. This law is less regular than the Gaussian function because its derivative is not continuous at $x^2 + y^2 = L/2$. This renders this case slightly more

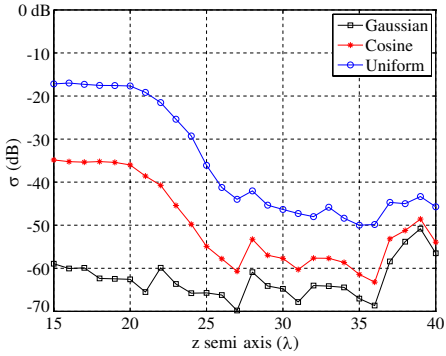

Figure 10. Influence of the excitation and of the z semi-axis on the expansion accurary.

difficult to tackle when the expansion surface is very near the planar aperture. The uniform law, that presents a discontinuity at its edges, confirms that irregular laws are more difficult to expand when the expansion surface is very near the aperture. The use of a smaller value of d would decrease this error, but it would increase the number of beams.

4.4. Computation of the Field Radiated from (S)

In Section 3.2, we have presented an example of CGB and we have tested its analytic formulation. In Section 4.2, we have shown that in various configurations the expansion parameters can be chosen so as to achieve a small error in the expansion at the expansion surface.

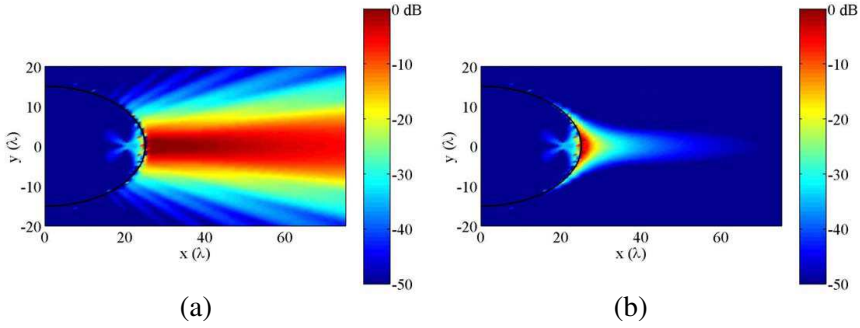

Figure 11. Electric field **E** in the near field zone: (a) CGB summation, (b) difference with the reference.

Now, we analyze the ability of our technique to compute the fields radiated from the expansion surface at any point of space. To do so, we add the contribution of all the CGBs produced by the expansion by means of their analytic formulation valid at great distances. The result of this simulation with the parameters $d = W_0 = \lambda$ is depicted in the plane $y = 0$ in Fig. 11. We note very small differences with the reference solution (numerical computation of the radiation integrals) at every computation points, except very close to the surface. In this area, the great distance approximation used to obtain the formulation of the CGB is no longer valid.

5. CONCLUSION

In this article, we have proposed an expansion technique to express the radiation of electric/magnetic currents known on a curved interface with a set of elementary beams, the conformal Gaussian beams. They correspond to the radiation of elementary currents which locally have a Gaussian amplitude and a linear phase. They are characterized by a reference frame, a phase vector, and a complex curvature matrix.

In the expansion we have chosen these parameters to obtain an accurate description of the problem with a reduced number of elementary beams. The beams are placed on a regular mesh of the curved interface. Symmetric Gaussian functions are used. The phase vector is determined so that it respects the local physical properties of the current to be expanded. We have employed a point matching technique to compute the expansion coefficients. We have ended up with four linear systems, which solutions only involve one LU decomposition.

We have proposed an analytical formulation for conformal Gaussian beams by means of an asymptotic evaluation of the radiation integrals valid at great distances. An example has been introduced, from which the analytical formulation has been confronted to the reference solution with satisfying precision.

Finally, we have conducted numerical tests on the expansion and explained how the expansion parameters can be chosen so as to obtain an accurate description of the currents with a moderate number of beams. We have also shown that the configuration may play a role in the expansion accuracy. Very irregular currents may decrease the accuracy of the expansion. At every computation points except very close to the interface, the radiation has been accuratly computed by adding all the CGBs produced by the expansion via their analytic formulation.

This new expansion may be of interest to compute the radiation

pattern of antennas protected by sharp nose aircraft radomes [16]. Indeed, such an application requires an expansion that is less limited in terms of incidence and curvature than the one presented in [5].

An important extension for this work would be to find an analytic formulation of CGBs valid at any distance. A solution may consist in using the plane wave spectrum of CGBs introduced in [17], or alternatively in performing an asymptotic evaluation of the radiation integrals with another approximation such as the paraxial approximation. Another extension would be to develop an asymptotic formulation for the reflexion/transmission of a CGB at a metallic or dielectric interface as it exists for fundamental Gaussian beams [3, 19]. This would lead to a beam tracking algorithm based on CGBs.

REFERENCES

1. Kogelnick, H. and T. Li, "Laser beams and resonators," *Proceedings of the IEEE*, Vol. 54, No. 10, 1312–1329, 1966.
2. Sokoloff, J., S. Bolioli, and P. F. Combes, "Gaussian beam expansion for radiation analysis of metallic reflectors illuminated under oblique incidence," *IEEE Trans. on Mag.*, Vol. 38, No. 2, 697–700, 2002.
3. Chou, H. T., P. A. Pathak, and R. J. Burkholder, "Novel Gaussian beam method for the rapid analysis of large reflector antennas," *IEEE Trans. on Antennas and Propag.*, Vol. 49, No. 6, 880–893, 2001.
4. Pascal, O., F. Lemaître, and G. Soum, "Dielectric lens analysis using vectorial multimodal Gaussian beam expansion," *Ann. Telecom.*, Vol. 52, No. 9–10, 519–528, 1997.
5. Chabory, A., J. Sokoloff, S. Bolioli, and P. F. Combes, "Computation of electromagnetic scattering by multilayer dielectric objects using Gaussian beam based techniques," *C.R. Phys.*, No. 6, 654–662, 2005.
6. Maciel, J. J. and L. B. Felsen, "Gabor-based narrow-waisted Gaussian beam algorithm for transmission of aperture-excited 3D vector fields through arbitrarily shaped 3D dielectric layers," *Radio Science*, Vol. 37, No. 2, vic6.1–6.9, 2002.
7. Galdi, V., L. B. Felsen, and D. A. Castanon, "Quasi-ray Gaussian beam algorithm for time-harmonic two-dimensional scattering by moderately rough interfaces," *IEEE Trans. on Antennas and Propag.*, Vol. 49, No. 9, 1305–1314, 2001.
8. Elis, K., A. Chabory, and J. Sokoloff, "3D interaction of Gaussian beams with dichroic surfaces for the modeling of quasi optical

systems," *International Symposium on Antenna Technology and Applied Electromagnetics (ANTEM)*, 1–5, Toulouse, France, June 2012.

9. Ghannoum, I., C. Letrou, and G. Bauquet, "Frame based Gaussian beam bouncing," *URSI International Symposium on Electromagnetic Theory*, 68–71, 2010.
10. Bogush, A. J. and R. E. Elkins, "Gaussian field expansions for large aperture antennas," *IEEE Trans. on Antennas and Propag.*, Vol. 34, No. 2, 228–243, 1986.
11. Einziger, P. D., Y. Haramaty, and L. B. Felsen, "Complex rays for radiation from discretized aperture distributions," *IEEE Trans. on Antennas and Propag.*, Vol. 35, No. 9, 1031–1044, 1987.
12. Casaletti, M. and S. Maci, "Aperture beam expansion by using a spectral 2D-GPOF method," *Progress In Electromagnetics Research M*, Vol. 28, 245–257, 2013.
13. Imbriale, W. A. and D. J. Hoppe, "Recent trend in the analysis of quasioptical systems," *Millennium Conference on Antennas and Propagation*, Davos, Switzerland, 2000.
14. Chabory, A., J. Sokoloff, and S. Bolioli, "Novel Gabor-based Gaussian beam expansion for curved aperture radiation in dimension two," *Progress In Electromagnetics Research*, Vol. 58, 171–185, 2006.
15. Chabory, A., J. Sokoloff, and S. Bolioli, "Physically based expansion on conformal Gaussian beams for the radiation of curved aperture in dimension 2," *IET Microw. Antennas Propag.*, Vol. 2, No. 2, 152–157, 2008.
16. Chabory, A., "Modélisation électromagnétique des radômes par des techniques basées sur les faisceaux Gaussiens," Ph.D. Thesis, Université Paul Sabatier, Toulouse, France, 2004.
17. Hillairet, J., J. Sokoloff, and S. Bolioli, "Electromagnetic scattering of a field known on a curved interface using conformal Gaussian beams," *Progress In Electromagnetics Research B*, Vol. 8, 195–212, 2008.
18. Felsen, L. B. and N. Marcuvitz, *Radiation and Scattering of Waves*, Electrical Engineering Series, Prentice Hall, Inc., 1973.
19. Chabory, A., J. Sokoloff, S. Bolioli, and K. Elis, "Application of Gaussian-beam based techniques to the quasi-optical systems of radio frequency radiometers," *European Conference on Antennas and Propagation (EUCAP)*, 1–5, Barcelona, Spain, April 2010.